Focus : the critical parameter for submicron optical lithography :part 2

William H. Arnold

Advanced Micro Devices
901 Thompson Place, MS 79, Sunnyvale, Ca. 94088

Harry J. Levinson

Sierra Semiconductor
2075 N. Capitol Ave., San Jose, Ca. 95132

Abstract

Depth of focus requirements and contributions to the focal error budget for submicron optical lithography are reviewed. Models are presented which estimate depth of focus in both thin and thick layers of photoresist. The effects of resist refraction on usable depth of focus are considered. Measurements of image plane tilt, curvature, and astigmatism in 5X reduction lenses collected using an automated, in situ, aerial image monitor are analyzed.

Introduction

Optical lithography is the key process technology which drives the capabilities of modern integrated circuits. The demand for greater device packing density and smaller features has been largely met by a succession of higher numerical aperture microlithographic lenses. The newest of these lenses have focal depths of about +/- 0.75 micron, comparable to the combined best control available for wafer flatness, device topography, and autofocus precision. As a result, it has become increasingly important to review precisely what impact wafer processing variables have on the usable depth of focus.

This paper continues where a previous paper left off[1]. First, linewidth change as a function of defocus and exposure using the thin resist model developed previously is calculated explicitly for the simple case of incoherent imaging near the resolution limit. Then, a thick resist model which takes into account bleaching upon exposure and development is introduced to estimate the impact of resist processing variables on usable depth of focus. The exposure model is exact in the limit that the resist contains no unbleachable component. The effect of contrast enhancing layers is easily incorporated. Linewidth, resist slope, and resist loss, which are independent parameters, are considered and a more rigorous definition of usable depth of focus is advanced. Results of the analysis are framed in terms of exposure/defocus (ED) diagrams, introduced by B. Lin[2-4].

The effects of refraction, which are appreciable for high numerical aperture optics, are found to reduce the limitations imposed by circuit topography. Wide field optics are constrained primarily by equipment manufacturing tolerances, wafer flatness, lens aberrations such as astigmatism and field curvature, and the effectiveness of the autofocus mechanism.Experimental data of submicron aerial image contrast as a function of defocus and field location showing curvature of the focal plane is presented. The data was collected using a Xerox Image Monitor invented by T. Brunner[5-7]. Several types of focusing and wafer leveling systems are reviewed. Wafer flatness requirements for submicron optical lithography are discussed.

Depth of focus in the thin resist model

The goal of this paper is to outline the effects of wafer processing variables on the usable depth of focus (DOF). In order to develop this theme, first considered is the ideal behavior of the aerial image incident in the wafer plane as a function of defocus. Initially neglected are all resist processing and wafer flatness variables. This will allow comparison between ideal behavior in thin resist and more realistic cases later.

In order to make the analysis simple, consider the incoherent imaging of an equal line and space grating of pitch P, linewidth L, and spacewidth W, P = L + W. The grating is imaged with diffraction limited optics at wavelength λ and numerical aperture NA. Only imaging near the resolution limit is considered so only the d.c. and first order spatial frequencies contribute to the image. This occurs when $P < 3\lambda/2NA$. In this case King's analysis[8] holds and the aerial image intensity is sinusoidal in the wafer plane:

$$I(x) = 1/2\ I_o\ [\ 1 + C(\Delta Z)\ \cos(2\pi x/P)] \qquad (1)$$

In Equation 1, I_o is the intensity in large open areas, x is the distance along the direction parallel to the wafer plane and cross-sectional through the grating (see Figure 1), and $C(\Delta Z)$ is the contrast of the aerial image as a function of defocus, ΔZ. The contrast of incoherent grating images at $P = 3\lambda/2NA$ is poorer than those produced with the partially coherent light normally used in optical lithography. As a result, simulated linewidth control and resist profile angles will be poorer than typically seen in practice. The purpose of using this model is to investigate the qualitative behavior of resist images as a function of defocus with relative mathematical ease, not to derive exact results.

Contrast is defined as

$$C = (I_{max} - I_{min}) / (I_{max} + I_{min}) \quad (2)$$

and is related to the incoherent modulation transfer function in this case by[8]

$$C(\Delta Z) = (4/\pi)\ MTF(\Delta Z) = (4/\pi)[1 - (4/\pi)\sin(\lambda/2NA\ P) - (2/3)(NA^3/\lambda P)\ \Delta Z^2\ ] \quad (3)$$

$$= C_o - D\Delta Z^2 \quad (4)$$

where C_o is the maximum contrast at zero defocus, Z_o, and D is a parameter which measures the curvature of the quadratic variation of image contrast with defocus. The resultant plot of image contrast versus defocus is a parabola with a maximum at (C_o, Z_o). At constant wavelength, a higher numerical aperture results in greater peak contrast and more pronounced curvature versus defocus.

As discussed in Part 1 of this paper (1), linewidth varies with focus quadratically in a thin resist model. In this type of model, all resist exposed to a threshold dose E_o and greater is removed upon development. Light absorption in the resist is ignored. An expression was derived which gives the linewidth change as a function of small changes in exposure and defocus:

$$\Delta x = \frac{\Delta E}{E}\left[\frac{1}{E}\frac{\partial E}{\partial x}\right]^{-1} - \frac{1}{2}\left[\frac{1}{E}\frac{\partial E}{\partial x}\right]^{-1}\left[\frac{1}{E}\frac{\partial^2 E}{\partial \Delta Z^2}\right]\ \Delta Z^2 \quad (5)$$

Substituting equations 1, 3, and 4 into this expression leads to

$$\Delta x = \frac{P}{2\pi}\left[\frac{\Delta E}{E}\ \frac{(1 + C_o\cos(2\pi x/P))}{C_o\sin(2\pi x/P)} - \frac{D}{C_o - D\Delta Z^2}\ ctn(2\pi x/P)\ \Delta Z^2\ \right] \quad (6)$$

The first term of equation 6 represents the linewidth change at zero defocus as a function of the fractional dose change, $\Delta E/E$. The second term represents linewidth change as a function of defocus, ΔZ. At the line edge $(x = P/4)$, the cotangent term is zero so x does not vary with ΔZ. The linewidth which is flat with defocus is called the isofocal or conjugate[9] linewidth . Thus, in this case, the isofocal linewidth is $P/2$. The term isofocal linewidth is used in this paper as it is more descriptive than conjugate width. The linewidth change Δx blows up as ΔZ approaches $\sqrt{C_o/D}$ so depth of focus is limited to $+/-\sqrt{C_o/D}$. It can be shown that this about $\sqrt{3}$ times the Rayleigh depth of focus, $+/-\lambda/2NA^2$.[8] Figure 2 shows an example calculated using equation 6 with NA = 0.45, λ = 0.436 micron, and P = 1.4 microns.

Linewidth as a function of image contrast, exposure, and defocus for incoherent imaging and a thin resist model has been calculated by C. Ausschnitt[10] by solving for x in eqn. 1 directly. The behavior of of his expression is very similar to that of eqn. 6.

B. Lin introduced the concept of exposure-defocus (ED) diagrams which represent the contours of maximum and minimum allowable linewidth as a function of exposure and defocus[2-4]. Lin used the full mathematical treatment of partially coherent imaging in the presence of defocus which yields more exact results than the simple treatment used here or in references (1) and (10), but explicitly ignored resist processing variables.

Linewidth as a function of exposure and defocus describes a curved surface. Slices through the surface parallel to the ED plane are taken at constant linewidth values. The projections onto the ED plane of the intersections of the slices with the curve make up the ED diagram. Projections of slices along the other two directions yield the more familiar linewidth vs. exposure or linewidth vs. defocus plots. ED diagrams neatly describe the process window within which it is possible to obtain linewidths within specified ranges. The concept can be extended to include further requirements on resist profile angle and top resist loss, as will be seen in the next section. ED diagrams for +/-10% linewidth contours have been calculated for two incoherent imaging cases and are

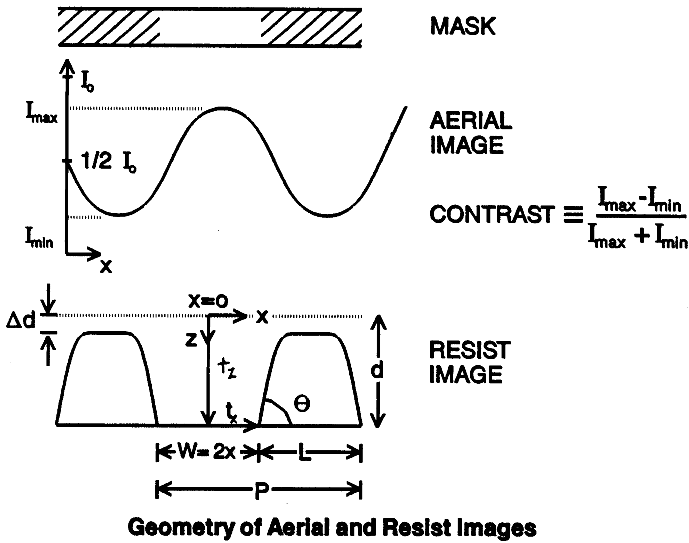

Figure 1. Geometry of aerial and resist images

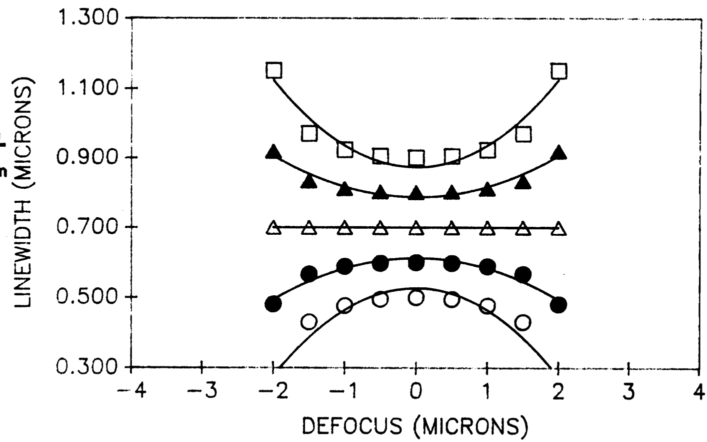

Figure 2. Linewidth vs. defocus using Eqn. 6.

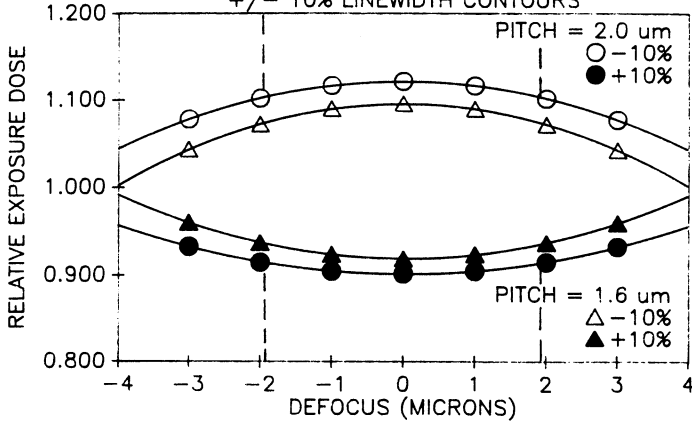

Figure 3a. ED diagram for incoherent imaging model. NA = 0.3, g line.

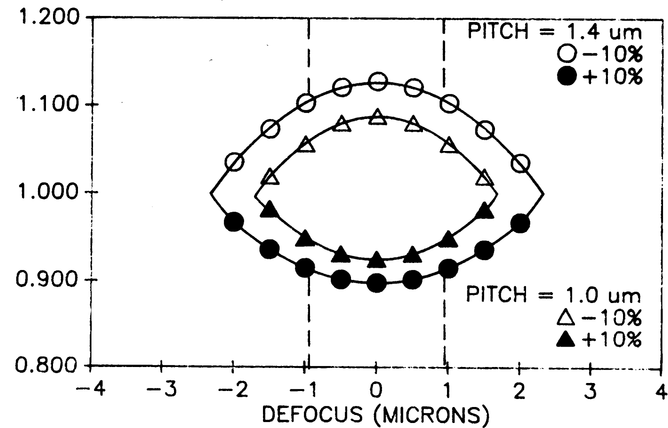

Figure 3b. NA = 0.45, g line.

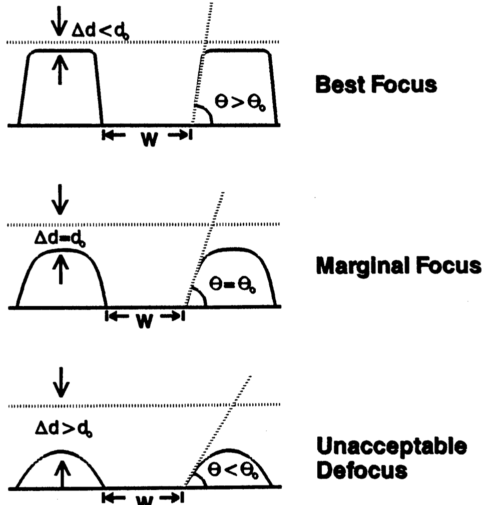

Figure 4. Even though all the images have the correct width at the base, resist loss from the tops of lines and the wall angle must also be in specification.

given in Figures 3a (NA = 0.3, λ=.436 um, P=2 and 1.6 um) and 3b (NA = 0.45, λ = .436 um, P=1.4 and 1 um). In these figures the axes have been rotated 90 degrees with respect to Lin's diagrams and both directions of defocus are considered in a manner recently developed by Ausschnitt[11]. Exposure doses are normalized to the exposure which produces equal lines and spaces.

It is worth examining these figures in some detail. The size of the ED window decreases with the pitch. The width of the window is a maximum at the nominal linewidth (L = P/2) for each pitch. This width is the depth of focus, $2\sqrt{C_o/D}$, which represents the physical limit of imaging with a thin resist capable of recording any nonzero contrast image. Typical resists require about 60% contrast for image transfer upon development. 60% contrast boundaries are shown in both Figures 3a and 3b. The depth of focus at any other exposure is the range of defocus which yields linewidths within the boundaries.

The exposure at which the linewidth contour is flat with defocus is termed the isofocal exposure. In this special case the isofocal linewidth is equal to the nominal linewidth. In the incoherent imaging, thin resist limit all size features reach nominal linewidth at the same exposure E_0, which is not the case with partially coherent imaging in thick resist. The height of the ED window at best focus is the exposure latitude.

Thick resist

While image contrast is probably the best single indicator of linewidth control[12], processing variables lead to significantly smaller usable focal depths than suggested by contrast information only. The ED windows presented in the previous section are artificially large because they represent ideal behavior at a single point in the image field, neglecting illumination nonuniformities, wafer flatness errors, image plane tilt, field curvature, astigmatism, resist processing and other effects encountered in practice.

Lithographers estimate the resolution and depth of focus from the Rayleigh resolution and depth of focus with appropriate scaling factors as $R = k\,\lambda/NA$ and $DOF = +/- K\lambda/NA^2$, where and NA are wavelength and numerical aperture, and k and K are the scaling factors. Combination of these two equations leads to an expression for DOF in terms of resolution and wavelength, $DOF = +/-(k/K^2)\ R^2/\lambda$. Rayleigh resolution, which strictly refers to the minimum separation between two coherent point sources which can be resolved, and Rayleigh depth of focus have the scale factor values k = 0.61 and K = 0.5, respectively. Lithographers estimate minimum resolution and DOF of resist images with k = 0.8 and K = 0.25 for single layer resist processes on low reflectance substrates. Advanced resist processes are assumed to decrease the resolution factor k, and to increase the DOF factor K. In order to demonstrate that the usable depth of focus is process dependent as well as being very sensitive to its detailed definition, a model is introduced which takes into account resist bleaching upon exposure and development through thick resist layers.

Consider the qualitative behavior of resist images in response to defocus. Defocus reduces the contrast of the aerial image. As a result, the slope of the image at the line edge decreases and the amount of light incident in nominally unexposed regions increases. These two effects lead to more sloped resist profiles and increased resist loss from the tops of features, both undesireable characteristics. This is illustrated in Figure 4. In the most important cases the resist sidewall angle and remaining thickness are as important for successful processing as is the line or the spacewidth, e.g., reactive ion etching of polysilicon gates in CMOS device fabrication. Thus a more rigorous definition of the depth of focus must also specify the minimum required resist wall angle, θ_0, as well as the maximum resist loss tolerable in nominally unexposed areas, Δd. Since the relative contrast of the resist process also directly impacts the resist wall angle and the unexposed resist removal rate, it follows that the usable depth of focus will also be directly affected.

By making simplifying assumptions, it is possible to reduce the equations which describe photoresist exposure and development given by Dill and coworkers[13] to forms which are more easily calculated than is done in the SAMPLE program[14]. This way, the particular optical and dissolution characteristics of a resist can be used directly to see their individual effects on DOF in certain ideal situations, with relative computational ease. The principal assumptions made, in addition to those made in the Dill model, are:

(1) Imaging takes place on a nonreflecting substrate;
(2) The nonbleachable absorption of the resist can be neglected throughout the exposure (i.e., B = 0);
(3) Development can be approximated as a two step process described by Greeneich[15] and Watts[16]. First calculated is the time to develop from the resist surface to the substrate at the image center, then the time to develop along the resist-substrate interface from the center to

any desired width is computed. The geometry is shown in Figure 1.

With assumptions (1) and (2), the coupled differential equations which govern the bleaching behavior of photoresist are

$$dI = - A M I_o dz \quad (7)$$

$$dM = - C I_o dt \quad (8)$$

where I_o is the light intensity in mW/cm2, M is the normalized photoactive compound concentration, A is the bleachable resist absorption before exposure in 1/um, C measures the relative photosensitivity of the resist in cm^2/mJ, z is the depth into the resist layer measured from the surface in um, and t is the exposure time in sec. These equations can be solved simultaneously to give[17-19]:

$$I(z,t) = I_o [1 - \exp(-CI_o t)(1 - \exp(Az))]^{-1} \quad (9)$$

$$M(z,t) = [1 - \exp(-Az)(1 - \exp(CI_o t))]^{-1} \quad (10)$$

which are respectively the light intensity at a depth z and at exposure time t and the corresponding photoactive compound concentration at that depth and time. An aerial intensity image $I(x,\Delta Z)$ is easily incorporated into these forms to give $I(x,z,\Delta Z,t)$ and $M(x,z,\Delta Z,t)$ by substituting I(x) for I_o in equations (9) and (10). Here z refers to the depth into the resist and Z to the amount of defocus.

In this formalism the exposure dose $E = E(x,z,\Delta Z)$ is calculated as

$$E(x,z,\Delta Z) = \int_0^t I(x,z,\Delta Z,t')\,dt' \quad (11)$$

$$= I(x,z,\Delta Z,t)t - \frac{Az}{C} - \frac{1}{C}\ln [1 - (1 - \exp(Az)\exp(-CI(x,z,\Delta Z,t)t))]$$

Note that the exposure dose coutours given by equation 11 do not coincide with either light intensity contours (eqn. 9) or photoactive compound contours (eqn. 10), except in the limit of long exposures.

In the approximation that development follows the contours of equal exposure dose, the resist sidewall angle as it meets the substrate can be evaluated at any exposure time. The tangent of the angle evaluated at (x,d) can be calculated as

$$\tan\theta = \frac{dz}{dx} = \frac{(\partial E/\partial x)}{(\partial E/\partial z)} = -\frac{Ct}{A}\,\frac{[1 - 2(1 - \exp(Ad))\exp(-CI(x)t)]}{[1 - (1 - 2\exp(Ad))\exp(-CI(x)t)]}\,\frac{dI}{dx} \quad (12)$$

This form of the wall angle shows it to be exposure dependent. In the limit of long exposures the term in the brackets goes to one and dz/dx goes to -(Ct/A)(dI/dx).

The Dill model relates the local development rate to the local photoactive compound concentration, described by the rate function R(M). A thin layer of resist dz is developed away in a time t = dz/R(M). The rate function used here is that of Kim et al[20], with parameters R1, the development rate for fully exposed resist in um/sec, R2, the rate for unexposed resist, and R3 is a dimensionless fitting parameter. No surface inhibition is assumed.

The time to develop through to the substrate at a depth z = d at the center of an image peaked at x = 0 can be calculated as

$$t_z = \int_0^d dz/R(M(0,z,t)) = (d/R_1) + ((1/R_2)-(1/R_1))\exp(-R_3)\int_0^d M(0,z,t)\exp(R_3M(0,z,t))dz \quad (13)$$

The time required to develop along the substrate starting at z = d out to a space edge position of x (total spacewidth W = 2x) is

$$t_x = \int_0^x dx/R(M(x,d,t)) = (x/R_1) + ((1/R_2)-(1/R_1))\exp(-R_3)\int_0^x M(x,d,t)\exp(R_3M(x,d,t))dx \quad (14)$$

The total develop time to reach a width W is then $t_{dev} = t_z + t_x$.

A computer program has been written for use on an IBM PC-XT which calculates spacewidth as a function of exposure and defocus at set d, A, C, R1, R2, R3, NA, λ, P, and develop time t_{dev}. The form of the aerial image is given by equation 1. ED diagrams have been constructed for three cases, in each a pitch is imaged by a lens with numerical

aperture sufficient only to pass the first order diffracted waves:

(1) NA = 0.30, λ = 0.436 um, P = 2.0 um
(2) NA = 0.45, λ = 0.436 um, P = 1.4 um
(3) NA = 0.35, λ = 0.248 um, P = 1.0 um

In each case the resist thickness was set equal to 1.0 micron. The resist and developer parameters used were A = 0.6 1/um, C = 0.01 cm^2/mJ, R_1 = 0.24 um/s, R_2 = 0.0001 um/s, R_3 = 6.1, representing a fairly typical g-line resist with a high contrast developer. Resists for case 3 (KrF excimer stepper) are unlikely to have such parameters but for the sake of consistency they were left equal to the g-line values. The diagrams are shown in Figures 5,6,and 7. The data points generated by the program for equal spacewidths are fit by fourth order regression.

It should first be noted that the nominal spacewidth (W = P/2) in each case is 0.2 to 0.35 um smaller than the isofocal width. Depth of focus as defined by +/- 10% of the spacewidth increases until the isofocal width is reached. Second, the behavior of the ED contours becomes increasingly pathological as defocus is increased, showing an inversion at doses comparable to or greater than the isofocal exposure. This inversion does not occur in the King model, which is manifestly quadratic in defocus.

A rigorous definition of DOF should include restrictions on resist profile and resist loss from the tops of images, as well as on space or linewidth. Contours of equal resist loss (8%, 10%, and 12%) for case 2 are shown in Figure 8a.

Contours of equal wall profile angle (70 and 75 degrees) for case 2 are shown in Figure 8b. These angles are calculated at the base of the developed image using eqn.12. This assumes that development follows the contours of equal exposure dose. The contours of equal wall profile in the ED plane are egg or raindrop shaped. Qualitatively, at small doses the wall profile is low because the aerial image has not sufficiently exposed the region near the line edge. As dose increases, definition of the line edge becomes sharper and wall angle increases. However, at high doses the wall angle peaks and starts to decrease because the line edge moves into regions of resist where there is less gradient between exposed and unexposed regions. Maximum wall angle in case 2 is 77 degrees at 1.3 times the replication dose and zero defocus. The low contrast of incoherent aerial images near $P = 3\lambda/2NA$ lead to poorer resist wall angle than seen in practice where one could expect $\theta > 85$ degrees for the same simulation parameters and a partial coherence factor of 0.5.

When spacewidth, wall angle, and resist loss contours are overlaid, a process window is formed in the area, if it exists, where all three sets of contours meet the requirements simultaneously (e.g., +/- 10% width, < 10% resist loss, > 75 degrees wall angle).

The process window so derived for case 2 is shown in Figure 9a, where the desired spacewidth is the same as the nominal, 0.7 um. The window is bounded in exposure by +/- 0.1 um width contours and by the 75 degree wall angle contour in defocus. All points in the window meet the 10% resist loss restriction. The depth of focus at 0.7 micron is about +/- 0.7 um. In Figure 9b the desired width is set at 0.8 um. It can be seen that the window is larger than in Figure 9a. The 10% resist loss contour bounds this window at the highest doses and defocuses. The depth of focus at 0.8 micron is about +/- 0.85 um. Thus, in this example, depth of focus can be increased by over 20% by exposing the spacewidth to 0.1 um larger than equal lines and spaces. This is an example of what is meant by masking bias: while it is possible to reproduce reticle features 1 to 1 (after reduction) on the wafer, there is in general both greater exposure latitude and usable depth of focus when the features are exposed beyond the replication dose.

There is a best numerical aperture to use to print a particular pitch. For a given pitch P, numerical apertures smaller than about $1.6\ \lambda/P$ will have image contrast too small to print. On the other hand, depth of focus shrinks rapidly as NA is increased. Thus one expects an optimum NA at which depth of focus is greatest for printing features of a certain size. One does not profit by using a high resolution lens when only moderate resolution is required because of the loss of depth of focus. Figure 10 shows depth of focus versus NA for a 2.0 micron pitch. Four different definitions of depth of focus generate the four different curves where the pitches are required to print down to equal 1.0 micron lines and spaces or to 0.9 micron lines, 1.1 micron spaces, and the wall profile is either 70 or 75 degrees. It can be seen that the best numerical aperture to use depends heavily on the exact resist image requirements. The simulation result that the best depth of focus is found when overexposure is used and the requirement on wall angle is relaxed satisfies the usual intuition.

Increasing contrast and edge sharpness of the aerial image will increase the subsequent resist line or space width control. A novel approach of increasing aerial image contrast photochemically was introduced by Griffing and West[21]. Contrast enhancement entails applying a very optically dense but extremely photobleachable film directly

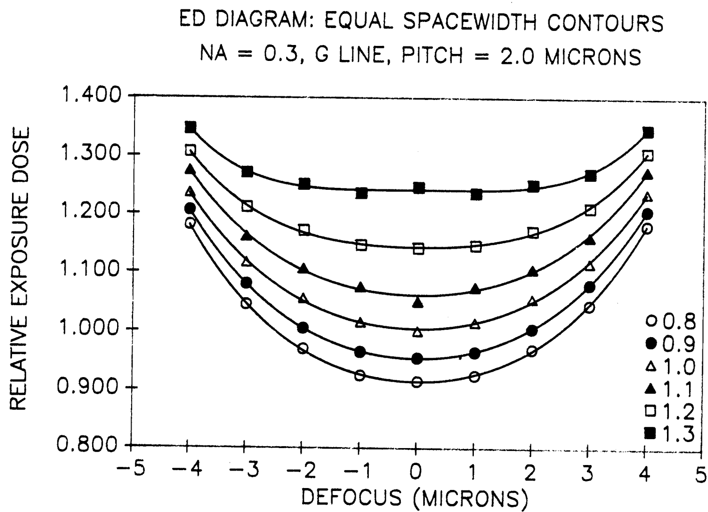

Figure 5. ED diagram. Incoherent imaging, 1.0 micron thick resist, NA = 0.3, P = 2 microns, g line.

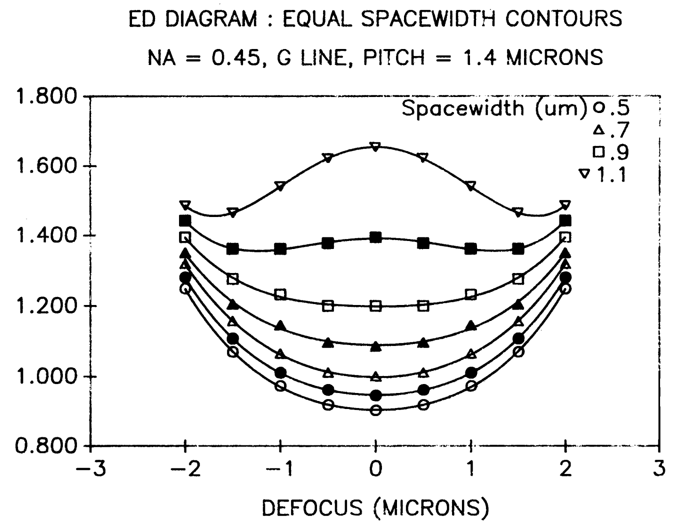

Figure 6. NA = 0.45, g line, P = 1.4 microns.

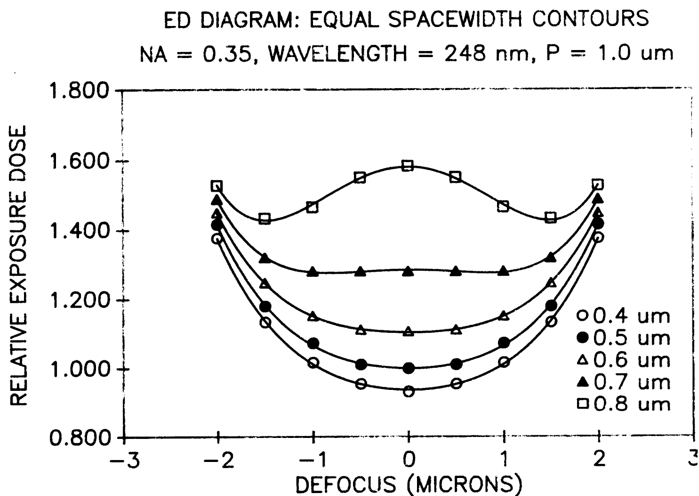

Figure 7. NA = 0.35, λ = .248 micron, P = 1.0 micron.

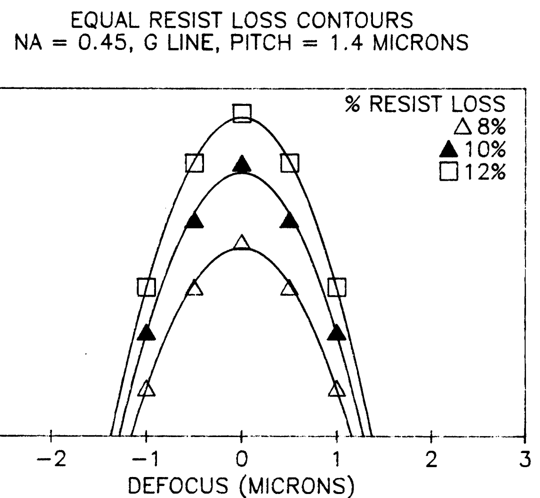

Figure 8a. Contours of equal resist loss from the tops of lines (8,10, 12% loss). Case 2 (Fig.6)

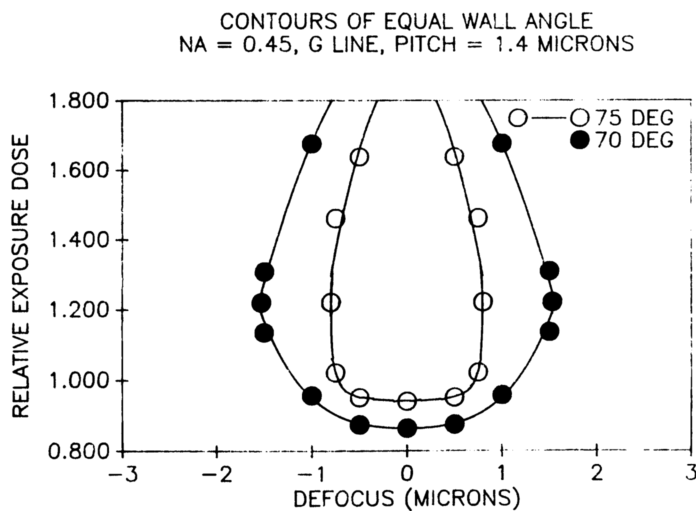

Figure 8b. (left) Contours of equal wall angle (70,75°). Case 2.

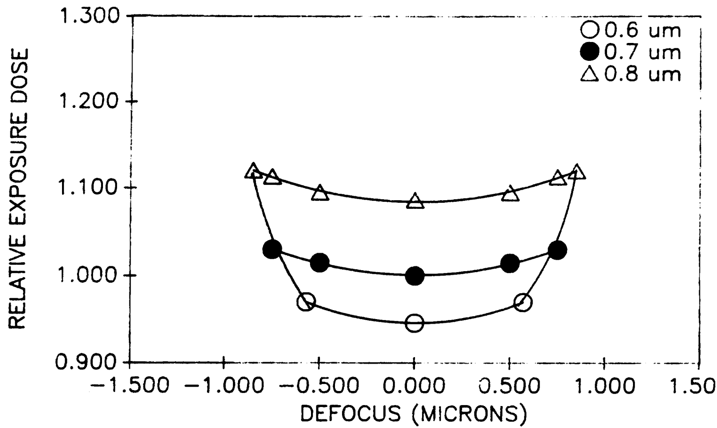

Figure 9a. ED process window. 0.7 +/- 0.1 micron, < 10% resist loss, > 75° wall angle. Case 2.

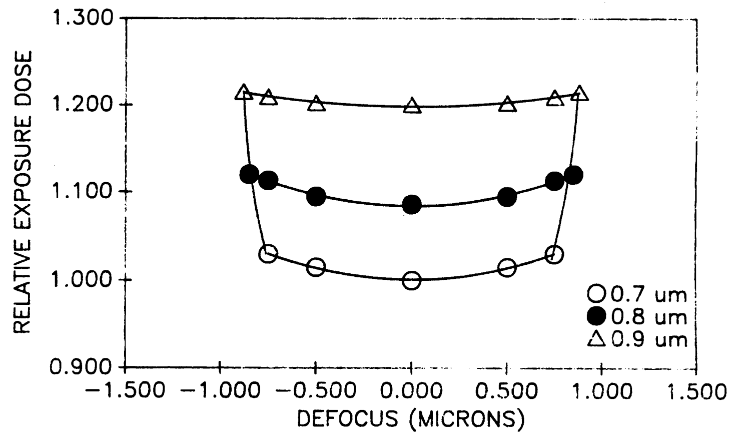

Figure 9b. ED process window. 0.8 +/-0.1 micron, < 10% resist loss, >75° wall angle.

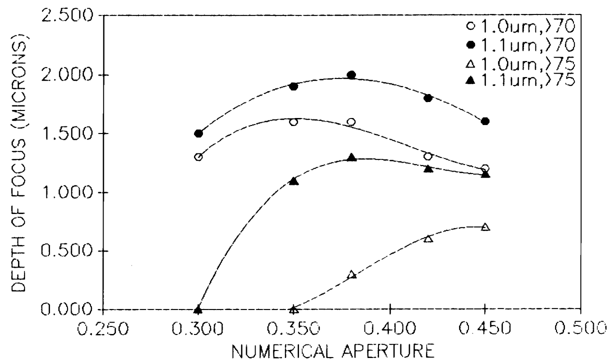

Figure 10. Depth of focus vs. numerical aperture. G line exposure, P = 2 microns.

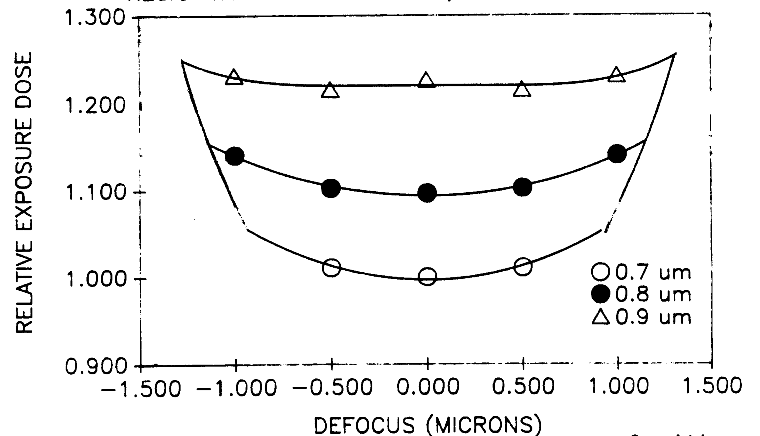

Figure 11. ED process window. Case 2 with contrast enhancement added.

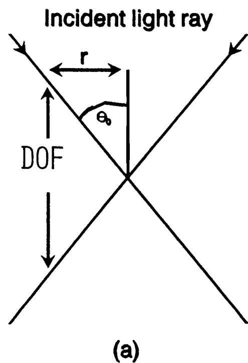

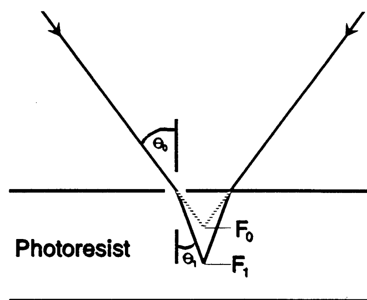

Figure 12a.
(left) Depth of focus in air (geometrical optics approximation.)
Figure 12b.
Depth of focus is modified by the resist layer with higher refractive index than air.

over the resist for exposure. Exposure bleaches the absorbing material over the nominal space and progresses into the resist while being effectively attenuated over the nominal line. With the proper choice of photobleaching materials, this can greatly increase the effective aerial image contrast and edge slope.

It is possible to incorporate contrast enhancement into the preceeeding model in a simple way. Assuming that the CEM can be characterized by A and C parameters[22], A_c and C_c and thickness d_c, then the effective aerial image incident on the resist surface is modified from $I(x,\Delta Z)$ to $I'(x,\Delta Z)$:

$$I'(x,\Delta Z) = I(x,\Delta Z)[1 - \exp(-C_c I(x,\Delta Z)t)(1 - \exp(A_c d_c))]^{-1} \quad (15)$$

To find the resultant intensity $I(x,z,\Delta Z,t)$ and photoactive compound concentration $M(x,z,\Delta Z,t)$ in the resist, one substitutes $I'(x,\Delta Z)$ for I_0 in equations (9) and (10) and all subsequent calculations proceed as before. Case 2 (0.8 micron desired space) was recalculated with a 0.5 micron thick contrast enhancing layer with parameters A_c = 10 1/um, and C_c = 0.1 cm^2/mJ and the results are shown in Figure 11. The maximum wall angle was 81.5 degrees, reached at 1.45 times the replication dose and zero defocus.

S. Lis has developed an empirical linewidth model which corresponds to the lowest order expansion of the incoherent imaging model[9,23]. Mack, Herschel, and Stephanakis have also presented a similar model[24].

Empirical ED diagrams can be derived simply from focus/exposure linewidth data[11]. The model described by equation 6 or by Ausschnitt's expression[10] can be used to generate a best fit surface.

Effects of refraction in the resist

The light energy which defines individual features must be well controlled throughout the thickness of the resist. For optics with low NA, the resist thickness is small compared to the depth of focus, so the light energy distribution may be calculated in a single plane and taken to be normally incident on the resist film. Accounting for the spatial variation in the light energy throughout the resist is reduced to considerations of absorption within the resist and reflections from the substrate, as is done in simulation programs such as SAMPLE.

For optics with large NA, rays of light which are not normally incident must be considered, and the contribution of the resist thickness must be determined. This is an extremely complicated problem, but some understanding may be achieved by considering the situation of thick resist and large angles of incidence in the context of geometrical optics. The focus of a point object is achieved in geometrical optics when all rays converge back to a point. Out of the plane of best focus, the image will form a circle of light. Within a particular context, a certain finite size of the image will be tolerable, and the maximum acceptable image radius will determine the depth of focus. The depth of focus for the aerial image can be seen from Figure 12a to be

$$DOF = 2r / \tan \theta_o \quad (16)$$

where θ_o is the largest angle of incidence, and is related to the numerical aperture by

$$\sin \theta_o = NA \quad (16')$$

A thin layer of resist, defined as one whose thickness is substantially smaller than DOF, can be placed within the region of acceptable focus, and the lateral light distribution is essentially that within a single plane. This is the situation described in most models. For thin resist layers, depth of focus is the distance over which the resist film can be moved and maintain feature sizes within specified tolerances.

When a thick layer of resist is placed near the plane of best focus, the effects of refraction must be considered. In Figure 12b two focused light rays which would converge to the point F_o if they passed completely through air would converge instead to the point F_1 because of refraction at the air-resist interface. The angles θ_o and θ_1 are related by Snell's law:

$$\sin \theta_1 = \sin \theta_o / n \quad (17)$$

where n is the refactive index of the resist. The resist thickness through which these light rays can pass before they diverge a lateral distance greater than 2r is increased from (eqn. 16) to

$$DOF' = 2r / \tan \theta_1 \quad (18)$$

This leads to an apparent increase in the depth of focus by a factor

$$\tan \theta_o \;/\; \tan \theta_1 \qquad (19)$$

For small angles, this is approximately equal to the refractive index of photoresist (n = 1.7 for typical positive resists at g line).

The depth of focus may be considered as follows. For any resist thickness, the focal range is defined as the distance over which the resist film may be moved and retain properly sized features. For thin resist films this will be related directly to the aerial image. For thick resist, part of the space within which rays remain adequately converged will be occupied by the resist. However, within the resist, the rays diverge less than in air. If DOF is the depth of focus for thin resist, then the focal range for thick layers is

$$DOF' = DOF - d/n \qquad (20)$$

where d is the resist thickness. The reduction of the depth of focus by the finite extent of the resist is decreased by the factor 1/n. A high index of refraction is desireable from the viewpoint of focus.

This effect might lead to asymmetrical behavior of linewidth versus defocus for high NA lenses. The range of defocus tolerable when focusing into the wafer would be expected to be about 1.7 times the range found when focusing away from the wafer if nominal best focus is placed at the resist surface. Thus a greater depth of focus is expected when the nominal best focus is set at the bottom of the resist layer rather than at the top.

Practical issues

There are numerous sources of focus error in stepper lithography. These errors can be grouped roughly under four general headings: errors due to the performance of the optics, those due to the automatic focus adjustment mechanism, those due to the nonplanarity of the wafer surface, and those due to the design and set-up of the stepper including the wafer chucking and leveling. There is no single plane in which all images come to focus because of field curvature, optical column tilt, and astigmatism. Likewise, the resist covered wafer surface does not present a planar surface on which to project the reticle image because of wafer flatness variations and circuit topography.

Measurement of focal plane flatness and astigmatism

Depth of focus is ultimately bounded by diffraction limited lens performance. In real stepper lenses, aberrations including astigmatism and field curvature degrade the usable depth of focus. Further, the mechanical set-up of the stepper in its manufacturing area is crucial as tilts in the optical column can cause the plane of best focus to be curved or inclined to the wafer surface.

Field curvature and astigmatism are present in very small amounts in the lens design but are increased significantly in the manufacturing process. One major lens manufacturer estimates that field curvature and astigmatism degrade the average lens performance by about one half a Rayleigh unit, in which about 30 to 40% is in the design and the rest is in manufacturing. Modern microlithographic reduction lenses include up to 20 separate glass elements, each surface of which can be ground to about $\lambda/20$ of the desired spherical form. Any cylindricity of these surfaces leads to increased field curvature and astigmatism. Field curvature can be largely corrected by adding shaped correction plates to the optical path. Astigmatism, present only in the corners of the field in design, is found even in the center of the field in real lenses and can only be reduced ultimately by grinding to finer tolerances than $\lambda/20$ [23].

At its simplest, the depth of focus of the lens can be defined as the range of defocus over which the image contrast is greater than a given minimum acceptable value. Indeed most lens manufacturers employ MTF testing as a function of defocus for both sagital and tangential directions using a variety of proprietary techniques. Minimum acceptable incoherent MTF is usually set at 45% (or about 60% contrast). This technique leaves much to be desired since it only measures the performance of the lens mounted on a test bench and not in the stepper in its final configuration. A technique invented by T. Brunner of Xerox PARC[5-7] allows direct measurement of a stepper's aerial image intensity in situ. As a result, contrast versus defocus can be measured in the real optical set-up at a number of points across the image field in both x and y directions.

Depth of focus must be defined so that it includes all points within the usable image

field since many devices will fail if a single logic gate is printed out of focus. While impressive depth of focus (as defined by the 60% contrast criterion) can be demonstrated at a single point in the image field, the lithography engineer must define depth of focus as the range over which images at all points in the field simultanteously not only meet the desired contrast criterion, but also produce high quality resist images.

That this is an important consideration is borne out in experimental data collected using a Xerox Image Monitor[5-7] on two GCA Model 6100 5X reduction steppers equipped with Maximus 600 illuminators and Zeiss 10-78-37 lenses (NA = 0.3, λ = .436μm). The experimental apparatus and technique were substantially the same as described in reference(7) with the exception that the reticle image was that of an isolated 3 bar pattern, a chrome line flanked by a window on either side, the image of each 0.8 micron wide at the wafer plane. Contrast was measured from the individual aerial image intensity profile traces (see Figure 13) and was defined as in Eqn. 2. Image contrast versus focus setting was measured at 5 points, center of the field and up, down, left and right, each 6.2 mm from center. Seven different focus settings were chosen using the stepper's nominal setting (as determined by inspection of resist images) as zero defocus.

An example of the data is shown in Figure 14 where contrast versus defocus is plotted for x and y directed 0.8 micron nominal lines measured at the center of the field of stepper #1. Both curves are fit with parabolas. They do not completely overlap, revealing an astigmatism. The 60% minimum contrast criterion was met over a range of about 3 microns. Similar curves were found at the other field locations. In contrast to the 3 micron dof at one point, the range over which all 5 locations, both X and Y directed pitches, simultaneously met the 60% criterion was found to be 1.25 microns on stepper #1 and only 0.5 micron on stepper #2, as shown in Figure 15. A different way of representing this data is shown in Figure 16 where the maximum and minimum contrast values found anywhere in the field at different focus settings are plotted. The usable depth of focus is determined from the minimum curve.

It should be noted that the Zeiss 10-78-37 lens is specified as a 1.1 micron resolution lens so that its performance is by no means optimized for work at 0.8 micron. Nevertheless, images near the Rayleigh resolution limit are the first to show the ill effects of aberrations or lens tilts. Similar full field contrast measurements for this lens at 1.0 and 1.2 micron feature sizes were reported by P. Chien, L. Liauw, and M. Chen[26].

Stability of focus setting

There are a number of ways that the stepper focus setting can vary from the value determined by testing at a previous time. It was reported in (1) that changes in barometric pressure can shift the plane of best focus by changing the refractive index of air. This was also reported in references (7) and (27). New steppers track barometric pressure and adjust the nominal focus setting either through software or by pressurizing the reduction lens. Also, the measurement error in determining the best focus setting is usually large in the absence of large numbers of real time precision measurements. Exhaustive measurements of linewidth control and resist wall angle using SEM is too slow for anything more than initial lens characterization. Focus setting is typically determined by inspection of a matrix of exposures at various focus settings and is largely a matter of judgement based on the behavior of resolution patterns such as small spots or gratings. In situ, automated aerial image sensing techniques such as the Xerox Image Monitor are needed in future optical systems in order to minimize this error, from greater than +/- 0.5 micron to +/-0.25 micron or less.

The autofocus adjustment system can also contribute to focus offset error. Wafer thickness and non-linear flatness variations, and circuit topography heights are typically much greater than the depth of focus so all steppers must incorporate a mechanism which senses the lens to wafer separation and adjusts it mechanically to maintain a constant gap at each exposure. At least three different techniques are employed to sense the wafer surface for automatic focusing in steppers. These techniques use infrared or laser beam reflectance, air pressure, or capacitive measurements.

IR beam reflectance autofocus is the most commonly used technique. In its simplest form, an infrared beam (700nm$< \lambda <$900nm) is reflected off the wafer surface at a glancing angle ($2^{\circ} < \theta < 20^{\circ}$) and is detected by a Si photodiode. The reflected beam is stronger and less sensitive to thin films when the angle is decreased. Wafer height displacements are transformed to lateral displacements (i.e., perpendicular to the optic axis) of the IR beam with respect to the fixed Si photodiode. The stepper adjusts the wafer-lens separation so that the IR beam remins centered on the detector. Early steppers moved the column up and down to adjust the gap, but most now move the wafer chuck instead since it is much less massive.

The IR autofocus scheme is subject to large focusing errors as a result of circuit

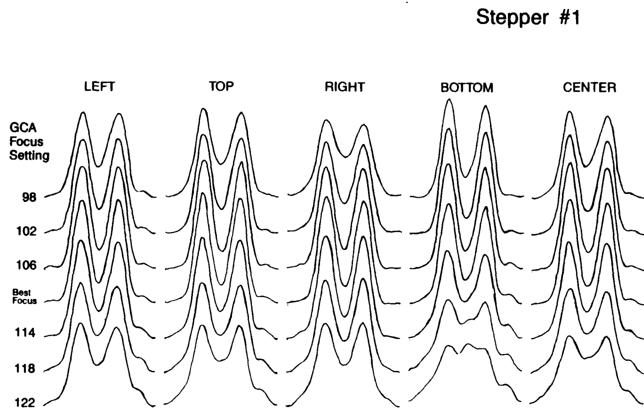

Figure 13. Experimental aerial image traces: Xerox Image Monitor. 0.8 micron line at various defocuses and field points.

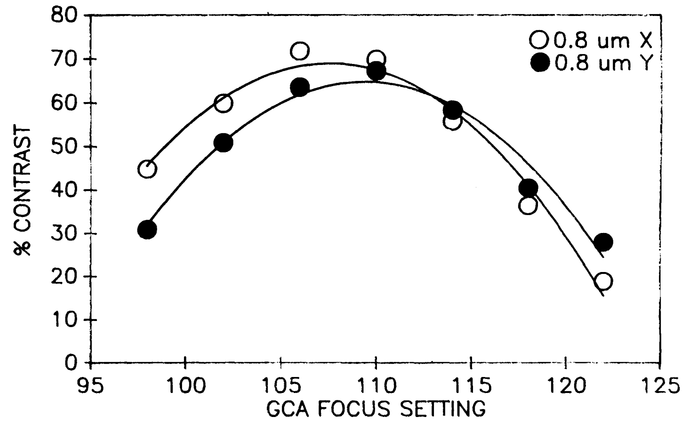

Figure 14. Contrast vs. defocus at the center of the field, X and Y geometries.

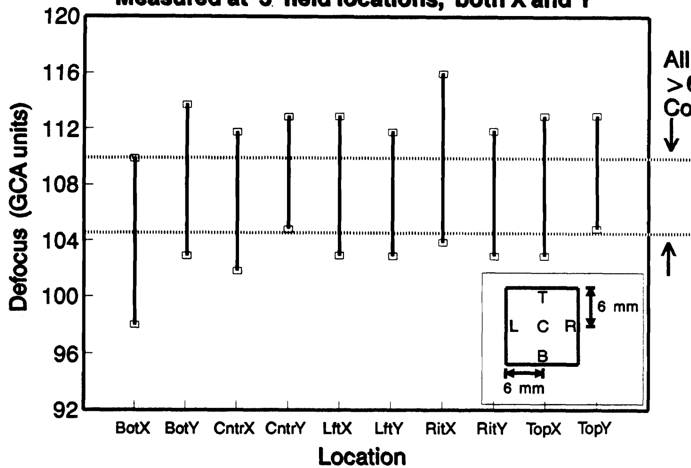

Figure 15a. 60% contrast range vs. defocus at five field locations. GCA #1.

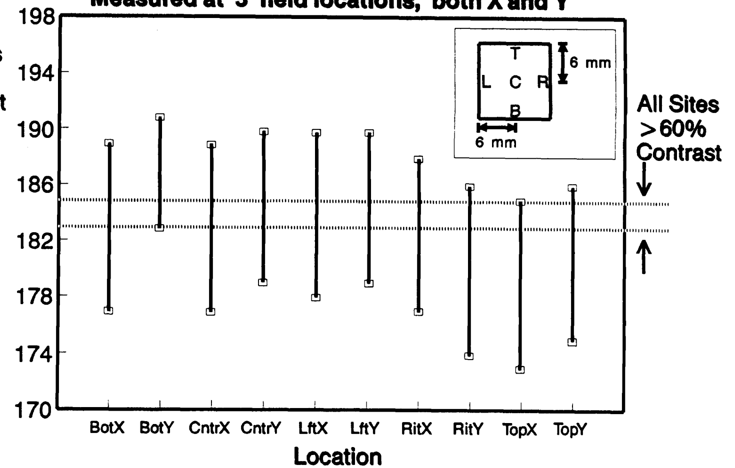

Figure 15b. 60% contrast range vs. defocus at five field locations. GCA #2.

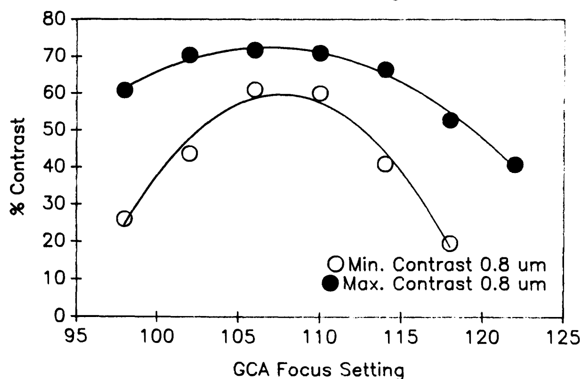

Figure 16. Maximum and minimum contrast found anywhere within the field vs. defocus. Depth of focus is determined by the range of the minimum curve.

Nonplanarity of Stepper Image Plane
Xerox Image Monitor Data -0.8µm Lines
Zeiss 10*78*37 5X, NA=0.3, λ=436nm

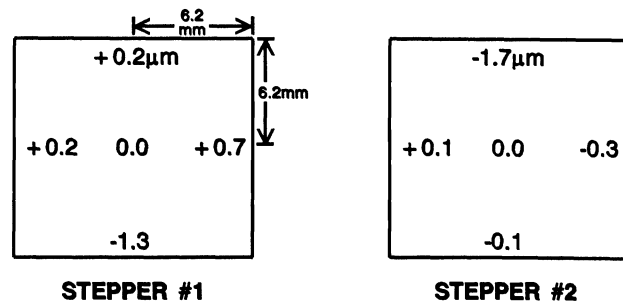

Figure 17. Best focus (in microns) at different field locations with the center set to zero.

topography[28] and infrared transmissive films[29] on the wafer such as resist and silicon dioxide. The intensity and position of the reflected beam as it strikes the detector can be shifted by thin film refraction and scattering from circuit topography. Newer systems have lower incident angles, orient the beam at 45 degrees to orthogonal topography and attempt to extract only the leading reflected beam from the wafer surface to minimize these problems.

Wafer surface sensing using air pressure is also widely employed. One commonly used stepper directs jets of pressurized air or nitrogen at three points surrounding the field to be printed and adjusts wafer height and tilt to equilibrate the pressure at the three locations. The gap between wafer and pressure sensor is very small (~40 microns). This technique has the advantage of being totally insensitive to thin film optical effects, sensing always the top surface of the wafer. However, environmental changes in barometric pressure or temperature will shift the nominal focus setting so constant monitoring and adjustments must be done. In addition, the presence of high pressure air jets tend to stir up any contamination already present in the system, so cleanliness is a key concern.

Capacitive measurements are also used on some steppers. Like air pressure autofocus, this technique requires a small sensor to wafer gap (also of order 50 microns).Likewise, capacitive measurements are thought to be relatively insensitive to the substrate under the resist layer, but since capacitance is determined from both geometry and the dielectric constants of the materials this needs to be proved unambiguously.

Wafer flatness and leveling

Wafer flatness variations can be grouped into linear and nonlinear errors. Linear errors, also called wedge or taper, can removed by wafer leveling. Nonlinear errors can not be compensated for and so must be controlled tightly by the silicon manufacturer. Nonlinear flatness errors are typically described in terms of the total included range (TIR) which is the difference between maximum and minimum wafer heights after wedge is removed. Currently, 150mm wafers can be procured which have TIR nonlinear flatness errors of less than 3 microns over the entire wafer surface (excluding a thin annulus at wafer's edge) with 98% of all 15 by 15 mm stepper fields within 1.0 TIR.

Most steppers in the field today use simple fixed wafer chucks which do not do any wafer leveling. More advanced designs level the wafer globally after taking a few autofocus measurements to determine the amount of wedge. In a further degree of sophistication, the stepper mechanically levels each field before exposure. Each successive refinement gives an increase in the effective depth of focus at the expense of increasing system complexity and reducing throughput.

Implicit in both wafer leveling and automatic focusing is the assumption of an algorithm which determines the particular tilt or height change to impart to the wafer at each field to minimize focus errors. What is the best ΔZ to employ as a result of n autofocus measurements? One might use the mean of the n measurements. Another approach might take the mean of the minimum and maximum data points. Since production lithography must image 100% of the field within the focal depth, the latter algorithm would be preferred since it is so heavily weighted by the height extremes. In the event that the differences between the extremes is greater than the focal tolerance, the stepper would use another less stringent algorithm to set the focal plane or skip the exposure altogether.

Focal error budget

Calculation of the total focal error budget will demonstrate how critical these issues are. Simple RMS estimates for the best available focal error control now and what will be required to achieve 0.5 micron optical lithography are listed below:

Wafer nonlinear flatness over field	+/- 0.50 um	+/- 0.30 um
Focus offset and autofocus precision	0.50	0.25
Circuit topography	0.50	0.10
Resist thickness (X 1/n)	0.30	0.15
Image plane flatness and astigmatism	0.50	0.30
	+/- 1.04 microns	+/- 0.52 micron

In order to meet +/- 0.5 micron depth of focus tolerances, the lithographer should plan to work on highly planarized surfaces in thin layers of resist. Super flat wafers will be required. Improvements will be needed in stepper autofocusing and in image field flatness.

Conclusions

Focus is the critical parameter for submicron optical lithography. As minimum feature sizes decrease and chip dimensions increase, no other parameter is so tightly squeezed as depth of focus. This paper has reviewed the impact which wafer processing variables and deviations from ideal lens performance have on usable depth of focus.

The usual definition of depth of focus as the range of defocus over which linewidth changes by less than +/- 10% must be upgraded to include minimum acceptable resist wall angle and maximum tolerable resist thickness loss from the tops of features.

Isofocal point processing is a key area for lithographers to investigate. Processes which have desired feature sizes at or near the isofocal point will have more process latitude. Shifting the position of the isofocal point by employing mask bias or by changing resist processing parameters can lead to significant increases in depth of focus. Exposure-defocus (ED) diagrams are an excellent graphic tool to visualize the lithography process window.

Focusing in thick resist probably leads to asymmetrical behavior with respect to the direction of defocus. Arguments advanced here lead to the conclusion that it is best to set nominal best focus at or near the bottom of the resist layer, rather than at the top.

There is a growing need for the capability to do rapid, exhaustive, and precise measurements of depth of focus. SEM measurements, while precise, are extremely slow and an exhaustive depth of focus evaluation for a single lens can take weeks to perform. We hope that the Xerox Image Monitor is the first of a succession of versatile, in situ stepper calibration equipment which will eventually lead to completely self-checking optical steppers.

Acknowledgements

We would like to thank Tim Brunner of Xerox PARC for the use of the Stepper Image Monitor. Helpful discussions with Kit Ausschnitt, Obelisk and Herman van Heek, ASM Lithography are greatly appreciated.

References

(1) H.J.Levinson, W.H.Arnold,J.Vac.Sci.Technol.B Vol.5,No.1,293(1987)
(2) B.J.Lin,IEEE Trans.El.Dev.,ED-27,No.5,931(1980)
(3) A.C.Liu,B.J.Lin,IEEE Trans.El.Dev.,ED-30,No.10,1251(1983)
(4) A.E.Rosenbluth,D.Goodman,B.J.Lin,J.Vac.Sci.Technol.B Vol.1,No.4,1190(1983)
(5) T.Brunner,R.R.Allen,IEEE El.Dev.Lett.,EDL-6,No. 7,329(1985)
(6) T.Brunner,R.R.Allen,SPIE Vol. 565,6 (1985)
(7) T.Brunner,S.M.Stuber,SPIE Vol. 633,106 (1986)
(8) M.C.King,"Principles of Optical Lithography", in VLSI Electronics Microstructure Science and Engineering Vol.1,N.G.Einspruch ed.(1981)
(9) S.Lis,SPIE Vol. 565, ,(1985)
(10) C.P.Ausschnitt,in VLSI Electronics Microstructure Science and Engineering, N.G. Einspruch,ed.,Vol.VIII,"Lithography for VLSI",R.K.Watts,ed.,Academic Press(1987)
(11) C.P.Ausschnitt:private communication. This approach is taken in Obelisk software.
(12) W.G.Oldham,S.Subramanian,A.R.Neureuther,Solid State Electronics,24,No.10, 975(1981)
(13) F.H.Dill, W.P.Hornberger,P.S.Hauge,J.M.Shaw,IEEE Trans. El.Dev., ED-22,445,(1975)
(14) W.G.Oldham,S.Nandgaodar,A.R.Neureuther,M.O'Toole,IEEE Trans. El.Dev., 26,717(1979)
(15) J.S.Greeneich,J.Appl.Phys,45,5264(1974)
(16) M.P.C.Watts,J.Vac.Sci.Technol. B 3(1),434(1985)
(17) H.C.Kessler,Jr.,J.Phys.Chem.,71,8,2736(1967)
(18) M.Kaplan,D.Meyerhofer,RCA Review,40,166(1979)
(19) A.V.Brown,W.H.Arnold,SPIE Vol.539,259(1985)
(20) D.J.Kim,W.G.Oldham,A.R.Neureuther,IEEE Trans.El.Dev., ED-21, 12,1730(1984)
(21) B.F.Griffing,P.West,Polymer Eng.Sci.,23,947(1983)
(22) M.O'Toole,IEEE Trans.El.Dev.Lett.,EDL-6,No.6,282(1985)
(23) S.Lis,Proceedings Kodak Microelectronics Seminar(1986)
(24) C.Mack, R.Herschel,A.Stephanakis,Proceedings Kodak Microelectronics(1986)
(25) H.van Heek, ASM Lithography: private communication.
(26) P.Chien,L.Liauw,M.Chen,SPIE Vol.538,197(1985)
(27) K.Hale, P.Luehrmann,Proceedings Kodak Microelectronics Seminar(1986)
(28) T.Herndon,C.Woodward,K.Konkle,J.Raffel,Proceedings Kodak Microelectronics Seminar (1983)
(29) J. Lavine,J.Vac.Sci.Technol.B Vol.5,No.1,304(1987)